Clinical Neurophysiology 121 (2010) 823–835

Contents lists available at ScienceDirect

Clinical Neurophysiology

journal homepage: www.elsevier.com/locate/clinph

Inferring spatiotemporal network patterns from intracranial EEG data ☆

A. Ossadtchi [a,*], R.E. Greenblatt [b,c], V.L. Towle [d], M.H. Kohrman [e], K. Kamada [f]

[a] Biology and Soils Department, St. Petersburg State University, Russia, Universitetskaya Emb. 7/9, St. Petersburg, Russian Federation
[b] Source Signal Imaging Inc., San Diego, CA, USA
[c] Computational Sciences Research Center, San Diego State University, San Diego, CA, USA
[d] Department of Neurology, Department of Surgery, Department of Pediatrics, Department of Psychiatry, The University of Chicago, Chicago, IL, USA
[e] Department of Pediatrics, The University of Chicago, Chicago, IL, USA
[f] Department of Neurosurgery, University of Tokyo, Tokyo, Japan

ARTICLE INFO

Article history:
Accepted 31 December 2009

Keywords:
Epilepsy
Network dynamics
Spatial dynamics
Seizure onset
Phase synchrony

ABSTRACT

Objective: The characterization of spatial network dynamics is desirable for a better understanding of seizure physiology. The goal of this work is to develop a computational method for identifying transient spatial patterns from intracranial electroencephalographic (iEEG) data.
Methods: Starting with bivariate synchrony measures, such as phase correlation, a two-step clustering procedure is used to identify statistically significant spatial network patterns, whose temporal evolution can be inferred. We refer to this as the composite synchrony profile (CSP) method.
Results: The CSP method was verified with simulated data and evaluated using ictal and interictal recordings from three patients with intractable epilepsy. Application of the CSP method to these clinical iEEG datasets revealed a set of distinct CSPs with topographies consistent with medial temporal/limbic and superior parietal/medial frontal networks thought to be involved in the seizure generation process.
Conclusions: By combining relatively straightforward multivariate signal processing techniques, such as phase synchrony, with clustering and statistical hypothesis testing, the methods we describe may prove useful for network definition and identification.
Significance: The network patterns we observe using the CSP method cannot be inferred from direct visual inspection of the raw time series data, nor are they apparent in voltage-based topographic map sequences.

1. Introduction

The epilepsies may be considered as a family of brain dynamics disorders (Kondakor et al., 2005; Hoke et al., 1989). These disorders may arise from a variety of underlying deficits, whose cellular physiology is still not well understood (Chang and Lowenstein, 2003) but which share an overlapping symptomatology. Often, the electrical disturbances appear to originate from a "focus", "epileptogenic zone" or "seizure onset zone", from which the disturbance propagates to other parts of the brain (Chang and Lowenstein, 2003), but defining and locating the epileptic network from interictal recordings remains elusive.

Most patients have a stereotyped seizure semiology, but may have variation of the electrocorticographic (ECoG) electrode site(s) at which paroxysmal activity starts (Bartolomei et al., 2000; Wennberg et al., 2002). This observation is consistent with the hypothesis that a network of cortical sites may be activated in order to initiate a seizure, but the excitation does not have to begin at a one fixed site within the network. Several studies (D'Alessandro et al., 2003, 2005; Mormann et al., 2003, 2005; Esteller et al., 2005; Le Van Quyen et al., 2005) have identified pre-ictal predictive information in recording sites remote from the seizure onset zone, consistent with an epileptogenic network model. Spencer (2002) and Bartolomei et al. (2000) have proposed several stereotyped epileptogenic networks (e.g., medial temporal/limbic, medial occipital/lateral temporal, superior parietal/medial frontal). Chaovalitwongse et al. (2008) hypothesize that seizure networks may develop pathologically from networks used for information coordination in the normal brain (Sporns and Kotter, 2004). In cases where the network model holds, this may suggest a surgical strategy sufficient to interrupt network connections by multiple subpial transection (Smith, 1998).

Methods for identifying networks inferred from iEEG recordings thus may have direct clinical value in presurgical evaluation and increase our understanding of seizure initiation and spread, with

☆ This work was supported in part by funding from the US National Institutes of Health.
* Corresponding author. Tel.: +7 921 427 2620.
E-mail address: ossadtchi@gmail.com (A. Ossadtchi).

1388-2457/$36.00
doi:10.1016/j.clinph.2009.12.036

implications for seizure prediction and control. Discrete networks may be characterized by correlation or synchrony of the electrical activity between the nodes that constitute the network. Thus, there has been considerable interest in the analysis of the ECoG recordings during the preictal, ictal, and postictal stages using correlation (Towle et al., 1999), phase synchrony (Nolte et al., 2008; Allefeld and Bialonski, 2007), and spatial complexity (Kondakor et al., 2005; Schindler et al., 2007) measures. Phase synchrony, in particular, is one of the most frequently used techniques to explore ECoG dynamics.

In this context, it is useful to distinguish between spatially non-specific and spatially specific synchrony measures that can be used to characterize a short segment of multichannel data. The spatially non-specific global synchrony measure is a scalar (usually between 0 and 1), e.g. (Schindler et al., 2007). The use of the scalar measure allows for estimation of the global synchrony and its evolution in time at the expense of spatial specificity.

Spatially specific synchrony measures estimate pairwise dependence between the signals at recording sites (Hoke et al., 1989). These measures are inherently spatiotemporal, and allow the investigator to trace explicitly the evolution of pairwise interactions in both time and space. However, visualization and interpretation are difficult because of the large amount of data generated to describe interaction between all pairs of recording sites for all points in time. For N recording sites and T time points, spatially specific synchrony measures are typically represented as a vector of matrices, and thus may grow as $O(N^2xT)$,

Here we propose some data reduction methods to facilitate an understanding of spatially specific synchrony measures. First we describe a simple method for reducing the array of matrices of synchrony estimates to a single matrix whose rows reflect the aggregate synchrony associated with the corresponding electrode. This view allows for a quick exploration of synchrony profiles, facilitating the visual identification of spatiotemporal patterns.

Next, we hypothesize that the process of seizure onset may be treated as an interplay of a small number of temporary quasi-stable networks. Synchronization between the neuronal populations serving as nodes of these networks yields a set of distinct synchrony profiles that can be observed when a suitable pair of recording sites is specified.

We present a method that leads to recovery of these transient networks and allows for reduction of the large amount of information generated from bivariate synchrony analysis. Our simple technique is based on the clustering of observed synchrony profiles, establishing the statistical significance of the clusters, and mapping back the composite synchrony profiles (CSP's) onto the electrodes by calculating the degree of involvement of each of the recording sites in each of the CSP's.

In principle, our data reduction technique does not depend on the specific method for bivariate synchrony analysis. For concreteness, however, we present the approach using the Phase Locking Value (PLV) synchrony measure. Bivariate PLV measures a signal property (phase locking between recording sites) that is expected to occur in spatial systems with coupled oscillatory dynamics. Alternative measures include correlation (Mormann et al., 2007), coherence (Towle et al., 1999), and mutual information (Chaovalitwongse et al., 2008; Pflieger and Greenblatt, 2005), among others (Mormann et al., 2007).

To validate the proposed approach we have used simulations as well as application of the methods to ECoG datasets recorded from three patients.

2. Methods

2.1. Phase synchrony estimation

In this presentation for concreteness we used phase locking value (PLV) (Hoke et al., 1989), as a measure of synchrony. The PLV is not affected by the difference in amplitude of the signals in the two channels and is sensitive only to phase locking. The PLV for a pair of channels is defined as the average length of the complex exponent vector raised to the power of instantaneous phase difference computed for the given pair of channels.

$$\mathrm{PLV}_{ij}(W) = \|E\{\exp(-i(\phi_i(t) - \phi_j(t)))\}\| \quad (1)$$

The instantaneous phase values $\phi_i(t)$ for the ith channel signal are extracted using Hilbert transform (Bracewell, 1986), where the expectation is computed over an interval τ_{PLV}. We note that instantaneous phase is well defined mathematically even for broadband signals, though the physical interpretation of broadband instantaneous frequency (the time derivative of the instantaneous phase) has been a topic of some debate (Cohen, 1995). To obtain an intuition into Eq. 1, note that when the phase difference between a pair of channels does not exhibit significant fluctuation the length of the averaged complex exponent vector remains close to unity. However, when the phase difference takes random values, the instantaneous complex exponent vectors point in random directions resulting into a nearly zero-length averaged complex exponent vector. Fig. 1 illustrates these ideas graphically. A more formal description can be found in Supplementary Appendix A.

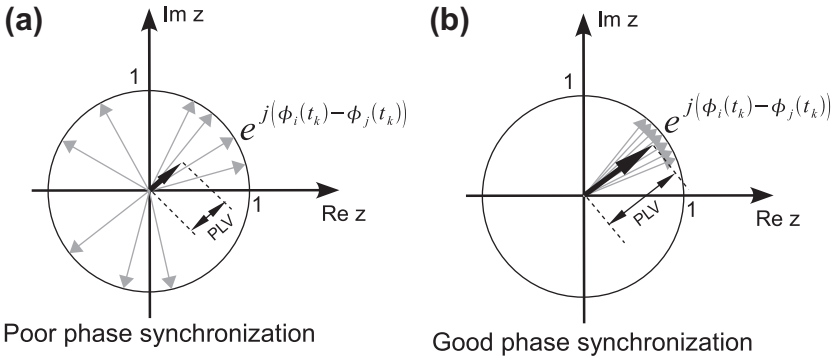

Fig. 1. The PLV for a pair of channels is defined as the average length of the complex exponent vector raised to the power of instantaneous phase difference computed for the given pair of channels. (a) Poor synchronization case, several instantaneous complex exponent vectors are shown in gray. In this case the phase difference tends to take random values and the instantaneous complex exponent vectors point in random directions uniformly distributed along the unit circle. The averaging of these instantaneous vectors results into a nearly zero-length vector shown in bold black and the length of this vector is the PLV metrics. (b) Shows several instantaneous complex exponents for the situation when the phase difference between the two channels appears to not significantly fluctuate around some constant value. The averaged vector remains of significance length close to unity.

Application of the PLV synchrony measure to the data with respect to a phase reference channel i_{ref} gives us the $N \times T$ PLV matrix $\mathbf{\Psi}_{i_{ref}}$ whose jth row corresponds to the phase synchrony temporal evolution of the jth and i_{ref}th channel time series. Note that the i_{ref}th row of $\mathbf{\Psi}_{i_{ref}}$ is identically unity. When we refer to the 'reference channel' in the PLV context, it should be clear that we refer to the phase reference channel and not the reference electrode that may be used for differential electrical recording.

For N channels and T time windows, the phase synchrony estimates may be stored conveniently as an array of N $N \times T$ matrices $\{\mathbf{\Psi}_{i_{ref}}\}, 1 \leqslant i_{ref} \leqslant N$.

2.2. Normed aggregate synchrony matrix

The normed aggregate synchrony (NAS) algorithm reduces the $N \times T$ matrix $\mathbf{\Psi}_{i_{ref}}$ into a scalar time series representing the degree of aggregate synchrony associated with each phase reference electrode i_{ref} and time t. We proceed by mapping each column of $\mathbf{\Psi}_{i_{ref}}$ into a scalar by computing the L_n norm of its column vector representation. The nth power of L_n norm of a vector $\boldsymbol{v}$ is defined as $(L_n(\boldsymbol{v})^n = \sum |v_i|^n$. To normalize the aggregate synchrony, the selected norm is then normalized by dividing by the number of non-reference channels, yielding a number between 0 (no synchrony) and 1 (complete synchrony). This yields the $1 \times T$ vector $\boldsymbol{s}^T_{i_{ref}}$, which represents the aggregate synchrony associated with i_{ref}th electrode as a function of time. We find empirically that the L_2 norm appears most useful for visual inspection of the resulting data. This is shown in Fig. 2. If we assume that each *column* of a reference specific PLV matrix $\mathbf{\Psi}_{i_{ref}}$ is represented by a vector in the N-dimensional space then the aggregate synchrony profile for this matrix is an $1 \times T$ vector with elements reflecting the length of the corresponding column of $\mathbf{\Psi}_{i_{ref}}$ in the N-dimensional space. This representation reduces a reference specific matrix $\mathbf{\Psi}_{i_{ref}}$ to a vector. The aggregate synchrony matrix consists of the vectors obtained from all reference specific matrices $\mathbf{\Psi}_{i_{ref}}$ for $0 < i_{ref} \leqslant N$. The rows of this aggregate synchrony matrix represent a measure of connectivity dynamics complexity associated with the corresponding electrode. The key steps of the NAS algorithm are illustrated in Fig. 3.

The NAS algorithm reduces the data to provide insight into connectivity dynamics, but does not reveal the spatial structures of the underlying networks. We next describe a second algorithm which addresses the network identification problem directly.

2.3. Phase synchrony networks from cluster analysis

We define an observable network operationally as a set of channels (i.e., spatial locations) with non-random dynamical interactions, as revealed by bivariate statistical measures (e.g., PLV). This implies that channels that participate in an observable network will show similar synchrony profiles, and that these profiles will differ from those of other networks, although channels may be members of more than one network, either simultaneously or successively.

These networks may be inferred from the array of PLV matrices $\{\mathbf{\Psi}_{i_{ref}}\}, 1 \leqslant i_{ref} \leqslant N$. To infer these networks from the data, we cluster the rows of each $\mathbf{\Psi}_{i_{ref}}$, keeping only those clusters that represent a limited number of distinct patterns, thus reducing matrix $\mathbf{\Psi}_{i_{ref}}$ to a few representative synchrony profiles. For clustering we used our subspace deterministic clustering method described in the next section. The final step of this clustering procedure is estimation of cluster significance under the null hypotheses of uniform scatter in the data dependent subspace. The details of statistical testing are given in Supplementary Appendix A and are illustrated in Fig. 4. This approach to treating the large amount of data generated by bivariate synchrony analysis is computationally feasible, while preserving the spatial information necessary for network identification. The utility of this approach is suggested by visual inspection of the synchrony matrices, where spatiotemporal patterns may be seen. One such matrix is shown in Fig. 5 where we can observe several pronounced temporal patterns that may be used to represent matrix $\mathbf{\Psi}_{i_{ref}}$ in a reduced form. Our final step finds the

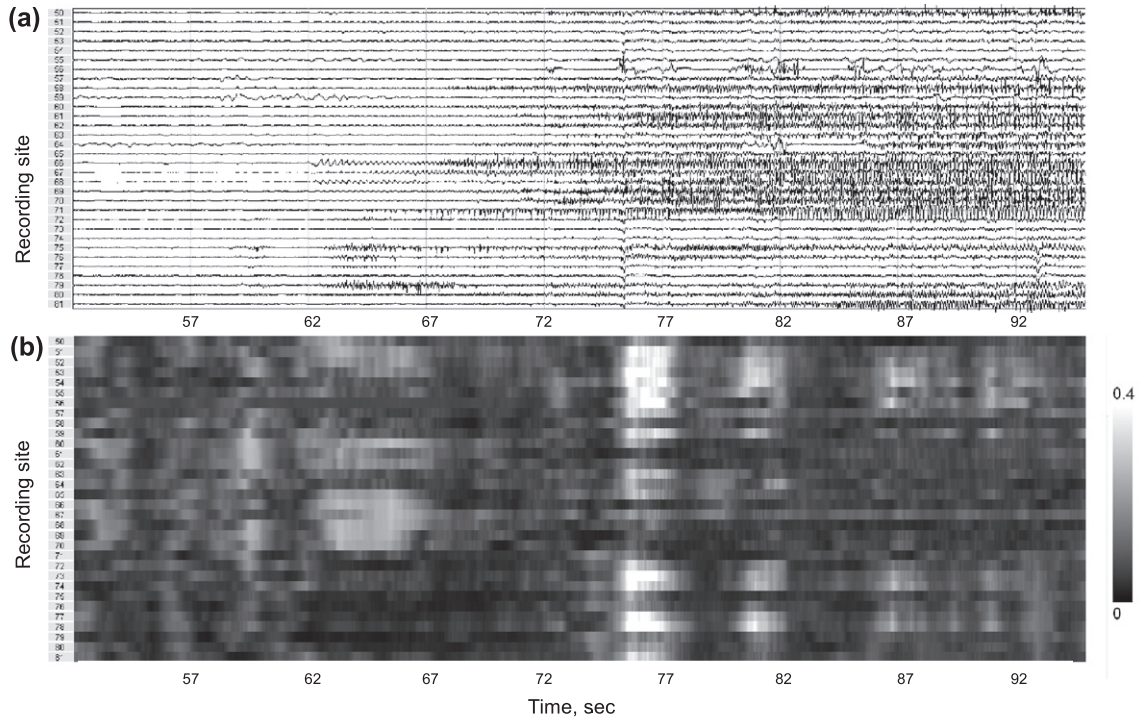

Fig. 2. (Top) A channel subset of ECoG data from patient 1 near the seizure onset is shown. This is the interval used for the analysis shown in Fig. 9. (Bottom) The L_2-normed aggregate synchrony matrix was computed for the channels and interval shown above.

composite synchrony profiles (CSPs) by applying the clustering procedure one more time to the rows of matrix $\overline{\Psi}$ containing most representative synchrony profiles for all recording sites used as a reference. We thus obtain K_o CSPs. We then test the hypotheses of the clusters being distinct using one-way multivariate analysis of variance (MANOVA). When the hypothesis of cluster similarity cannot be rejected, we merge the two clusters with the smallest Mahalanobis distance and repeat the test. We do so until we arrive to the final number of statistically distinct and significant K_f clusters represented in the form of a $K_f \times \widetilde{T}$ matrix Θ of K_f composite synchrony profiles.

The synchrony dynamics of the transient networks are characterized by K_f CSPs. In order to obtain spatial characteristic of the CSP specific networks we extract pseudo-topographies based on the following. The idea is to use a set of N PLV matrices $\overline{\Psi}_{i_{ref}}$ and match K_f extracted CSPs against the rows of these PLV matrices. The electrodes corresponding to the rows of the PLV matrices that sufficiently well match the kth CSP will contribute to the kth CSP topography. The diagram of the described CSP algorithm is presented in Fig. 6. The details of this procedure are described in Supplementary Appendix A.

2.4. Simulation studies

In order to validate the proposed approach, and also to understand its properties better, we performed a set of simulations. Using a nominal 10×10 electrode grid, we simulated non-stationary recording intervals to represent the transition to seizure dynamics. The details of the simulation algorithm are described in Supplementary Appendix B

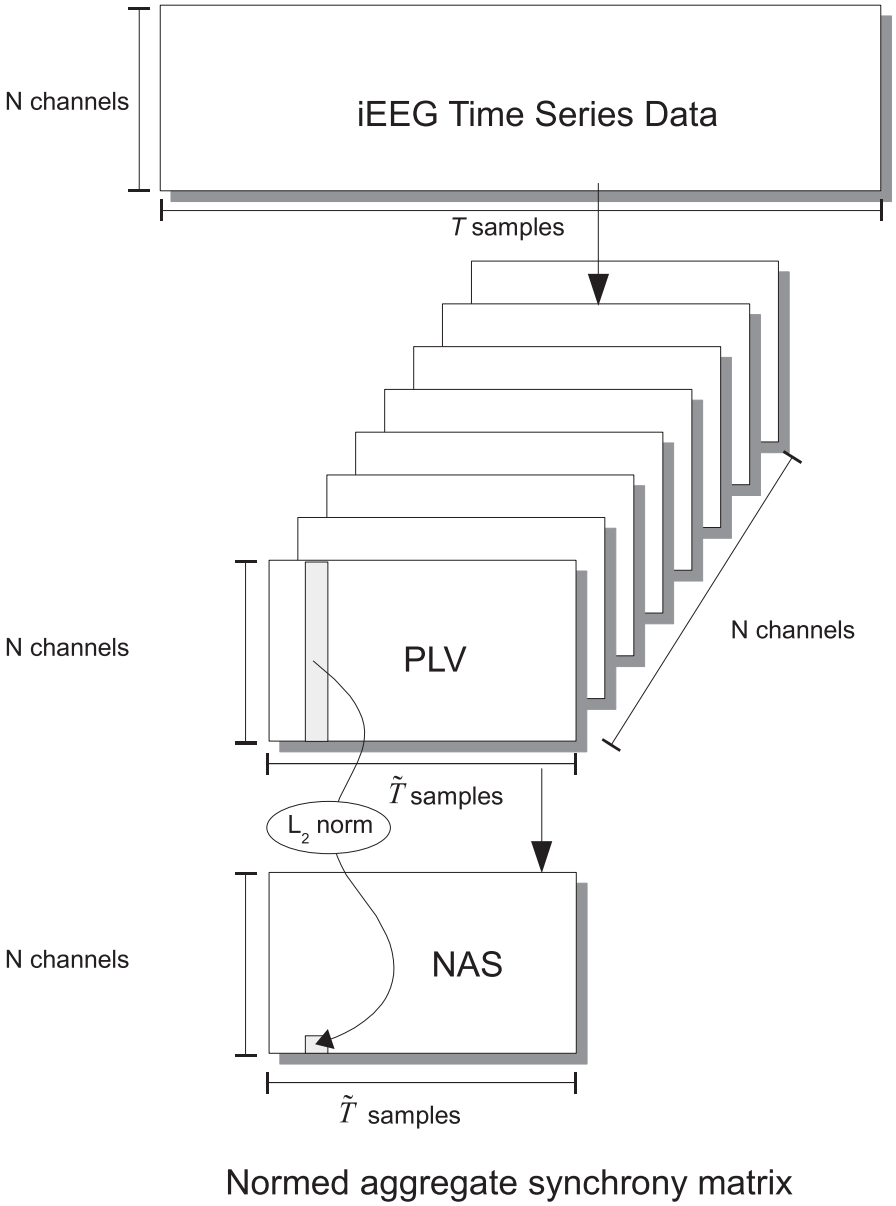

Fig. 3. Starting from the iEEG time series data for N channels and T time samples, the normed aggregate synchrony (NAS) algorithm algorithm first computes the phase locking variance (PLV) time series for each phase reference channel with respect to each of the other channels at a reduced effective sampling rate, $\widetilde{T}$. Each row of the NAS matrix corresponds to a phase reference channel. For each row of the NAS matrix, each element (time sample) represents the normalized total phase synchrony for that phase reference with respect to all other channels. Matrices are represented by rectangles. Although not drawn to scale, the relative rectangle sizes indicate the data reduction obtained as the algorithm proceeds.

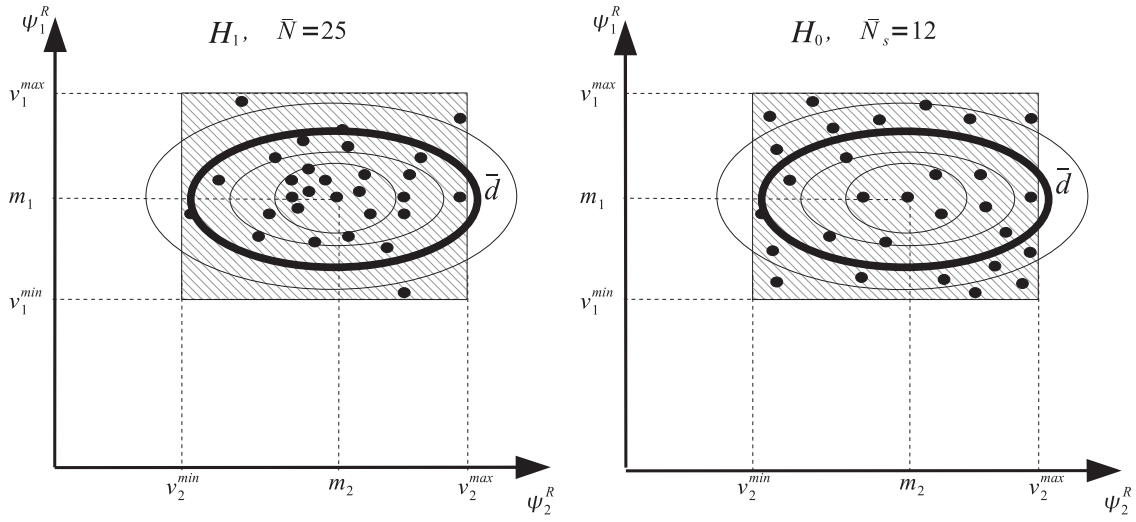

Fig. 4. Cluster significance is estimated by comparing the cluster data vectors to a surrogate distribution, as described in Supplementary Appendix A (*Establishing cluster significance*). Scatter plots of cluster datapoints are realized in the *R*-dimensional reduced space. $\boldsymbol{v}^{max} = [v_1^{max}, v_2^{max}]$ and $\boldsymbol{v}^{min} = [v_1^{min}, v_2^{min}]$ indicate the vectors defining the bounding rectangular volume (hatched) for the data vectors forming the cluster. These vectors determine the range of the *R*-variate uniform surrogate distribution used to test the cluster for significance by comparing the percentage of surrogate datapoints. The test is designed to count the percentage of datapoints from the surrogate distribution to appear within the 50% ellipsoid (shown in bold). On the left an example of a significant cluster is shown, for which we can not reject the H1 hypothesis as 25 out of total 29 points appear inside the ellipsoid. The right panel shows a set of 29 surrogate datapoints counting only 12 inside the ellipsoid corresponding to the average Mahalanobis distance for the cluster on the left panel.

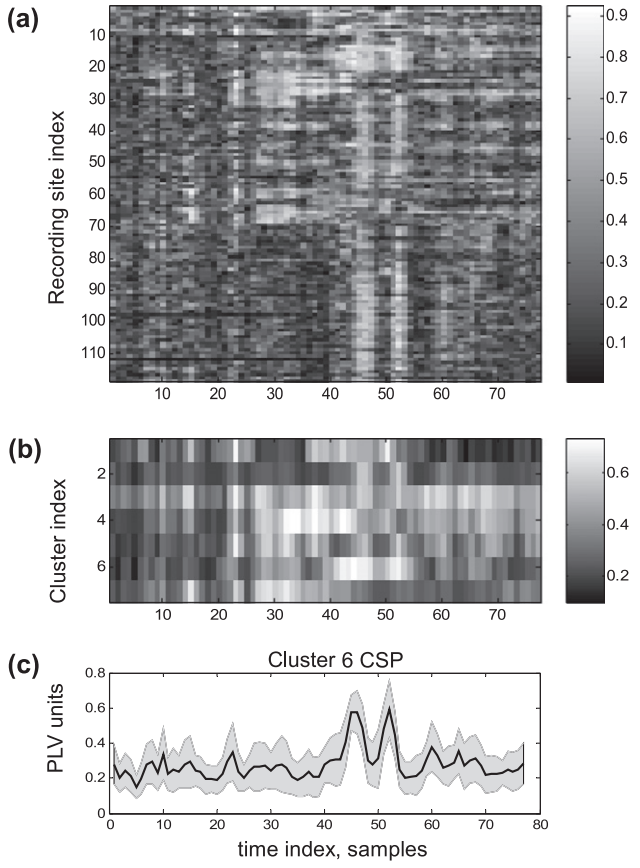

Fig. 5. (a) The PLV matrix (channel 1 phase reference) is shown for 80 s of ECoG data from the patient shown in Fig. 2. Several distinct temporal patterns may be seen (e.g., channels 14–20, 21–32, 84–112). The channels are ordered as in the original recording; they are not grouped by cluster. (b) Using PLV matrices for all channels as input data, seven statistically distinct clusters were obtained. The time course for each of the cluster centers is shown. (c) The mean ± standard deviation for cluster 2 is shown as a function of time. The mean and standard deviation summary statistics were obtained from the PLV time series for each of the reference-channel pairs identified as a member of this cluster.

3. Results

3.1. Simulation studies

As shown in Fig. 7, we were able to extract the principal profiles present in the simulated data. Our clustering procedure returned 3 clusters accounting for the data. Two of them were expected by the synchrony network construction (see Supplementary Appendix B). The third CSP's topography was spatially non-specific, involving all of the sensors to almost equal degree, and can be explained by the simulated surface conduction effect. The three clusters were found to be statistically distinct (MANOVA, $p < 1e-6$).

To assess the specificity of the proposed method we performed another set of simulations with no synchrony imposed on the simulated sources. The only potential synchrony source is due to the simulated surface conduction effect. The results of analysis of such dataset are shown in Fig. 8. CSP 1 is similar to the CSP 3 in Fig. 7 and reflects surface conduction effect. The topography of CSP 2 includes all sensors to almost an equal degree. This suggests the need for careful inspection of clusters that have both constant CSPs and topographies involving all of the sensors to essentially equal extent.

3.2. Patient data

We analyzed ECoG datasets including five seizures recorded from three patients, as shown in Figs. 9–11. Data were recorded at 400 Hz with respect to a scalp reference, and noisy channels (determined by visual inspection) were eliminated from further analysis. Patient data were obtained following all the guidelines for human subjects data required by the institutions with which the authors are affiliated.

Patient 1 was a 19-year-old male with a diagnosis of left temporal lobe epilepsy with pharmacoresistant complex partial seizures for 14 years. MRI demonstrated an abnormal high intensity in bilateral medial temporal regions, consistent with medial temporal sclerosis. Interictal ECoG found bilateral spikes, most frequent in the left temporal lobe. Many subclinical seizures were observed with frequent spikes in the left medial temporal region. At seizure

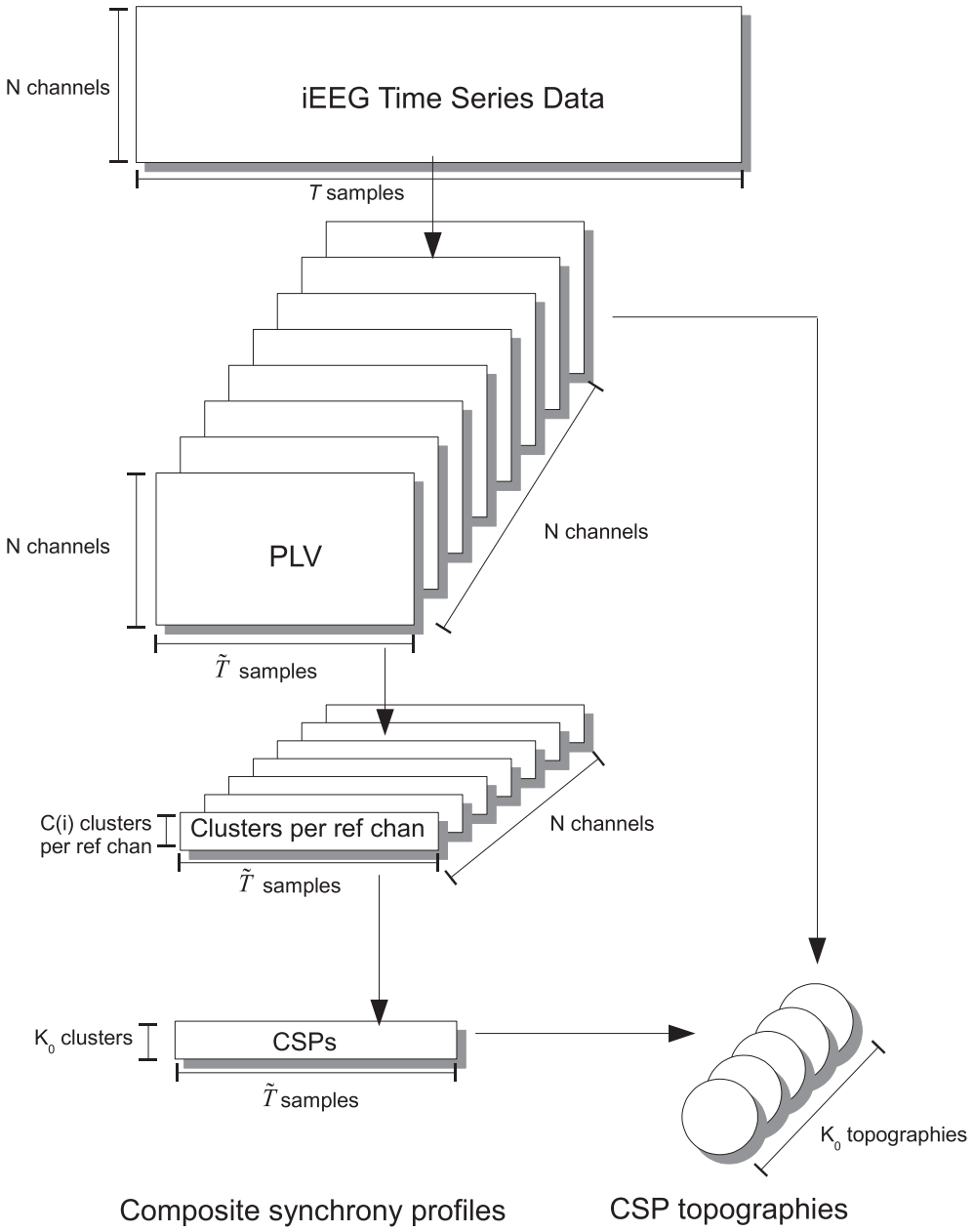

Fig. 6. Starting from the iEEG time series data for N channels and T time samples, the composite synchrony profile (CSP) algorithm first computes the phase locking value (PLV) time series for each phase reference channel with respect to each of the other channels at a reduced effective sampling rate. For each PLV matrix, the algorithm then determines a set of $C(i)$ statistically significant clusters separately for each phase reference i. This is followed by a second clustering step that finds K_0 statistically significant clusters over all phase reference channels. The second clustering step results in the composite synchrony profiles. These CSPs are then combined with the PLV data to infer the CSP topographies. Matrices are represented by rectangles, and topographies by circles. Although not drawn to scale, the relative rectangle sizes indicate the data reduction obtained as the algorithm proceeds.

onset, left and right medial temporal regions appeared to be simultaneously excited. Multiple subpial transection was performed in left hippocampus and left lateral temporal lobe (Shimizu et al., 2006). The patient has been seizure free with medication for over 18 months post-operatively.

Locations of 120 electrodes for Patient 1 were determined from post-operative CT and aligned to pre-operative volumetric MRI using EMSE v5.3 software (Source Signal Imaging, San Diego, CA). The estimated registration accuracy is ±2.5 mm, without accounting for surgical or MR imaging geometrical distortion.

Patient 2 was a previously normal 10-year-old right-handed female with a 2-year history of pharmacoresistant partial complex seizures with rare secondary generalizations. Chronic subdural grids were placed over the left frontal, parietal and temporal regions, and the right temporal lobe. Four days of monitoring revealed an epileptogenic focus in the left frontal and left parietal areas, which were resected. Pathologic specimens were consistent with cortical dysplasia. The patient had an Engel class 3 outcome, evaluated two years after surgery.

Locations of 102 electrodes for Patient 2 were determined from post-operative CT and aligned to the average brain (SPM) cortical surface using EMSE v5.3 software. Since subject-specific MR data was not used, this registration is approximate.

Patient 3 was a 14-year-old girl with neurofibramatosis and pharmacoresistant seizures. Chronic subdural grids and strips were place over left temporal, frontal, and parietal cortices. Seizure on-

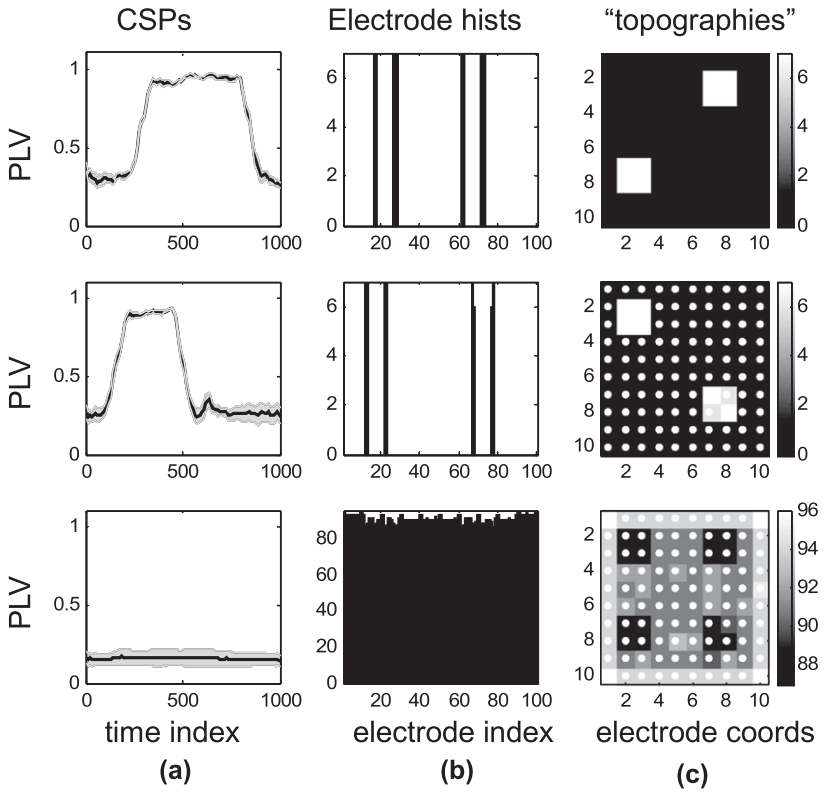

Fig. 7. Recovered synchrony profiles along with the topographies are shown for the simulated data that contained two synchrony bursts with overlapping temporal synchrony profiles represented by the two unit step functions active in the following intervals: network 1 (N1) 300–900 and network 2 (N2) 100–500 units of the time index. The topographies for N1 and N2 consisted of two nodes, each comprised of the four electrodes with the following coordinates N1: [(2-3,7-8) and (7-8, 2-3)], N2:[(2-3,2-3) and (7-8, 7-8)]. A graphical representation of the simulated data can be found in figure A1. The recovered profiles are shown in (a) and their topographies in (c). Two of the CSPs correspond to the simulated networks. The third CSP has small PLV values and corresponds to the simulated cortical volume conduction effect.

set was localized by inspection of the ECoG data to the left temporal lobe. A partial left temporal lobectomy, including mesial temporal structures, was performed. The patient had an Engel Class I outcome two years after surgery.

Locations of 88 electrodes for Patient 3 were determined using the methods described for Patient 2. The results were visualized on a representation of the brain surface, determined from post-implantation CT images.

Results for the normed aggregate synchrony measure are shown in Fig. 9(a) for Patient 1. Phase synchrony may be seen to increase at or near the seizure onset latency. It then declines during the seizure, and increases in the middle of the seizure. The re-

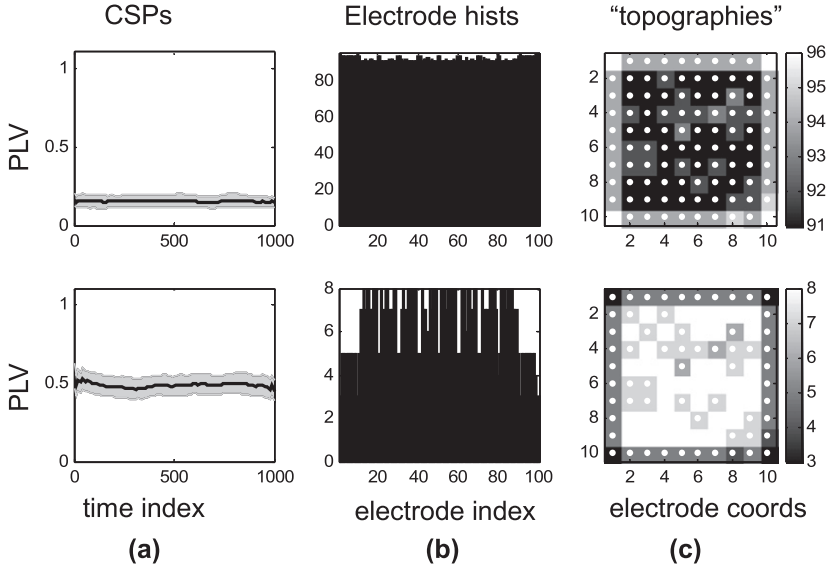

Fig. 8. Recovered synchrony profiles for simulations with no active networks present are shown. We tested the specificity of the proposed method by simulating the data that contains only surface conduction and no synchronous activity. The first synchrony profile is similar to the third profile in Fig. 7 and reflect cortical surface conduction effect. The second profile's topography engages all sensors to an almost equal degree.

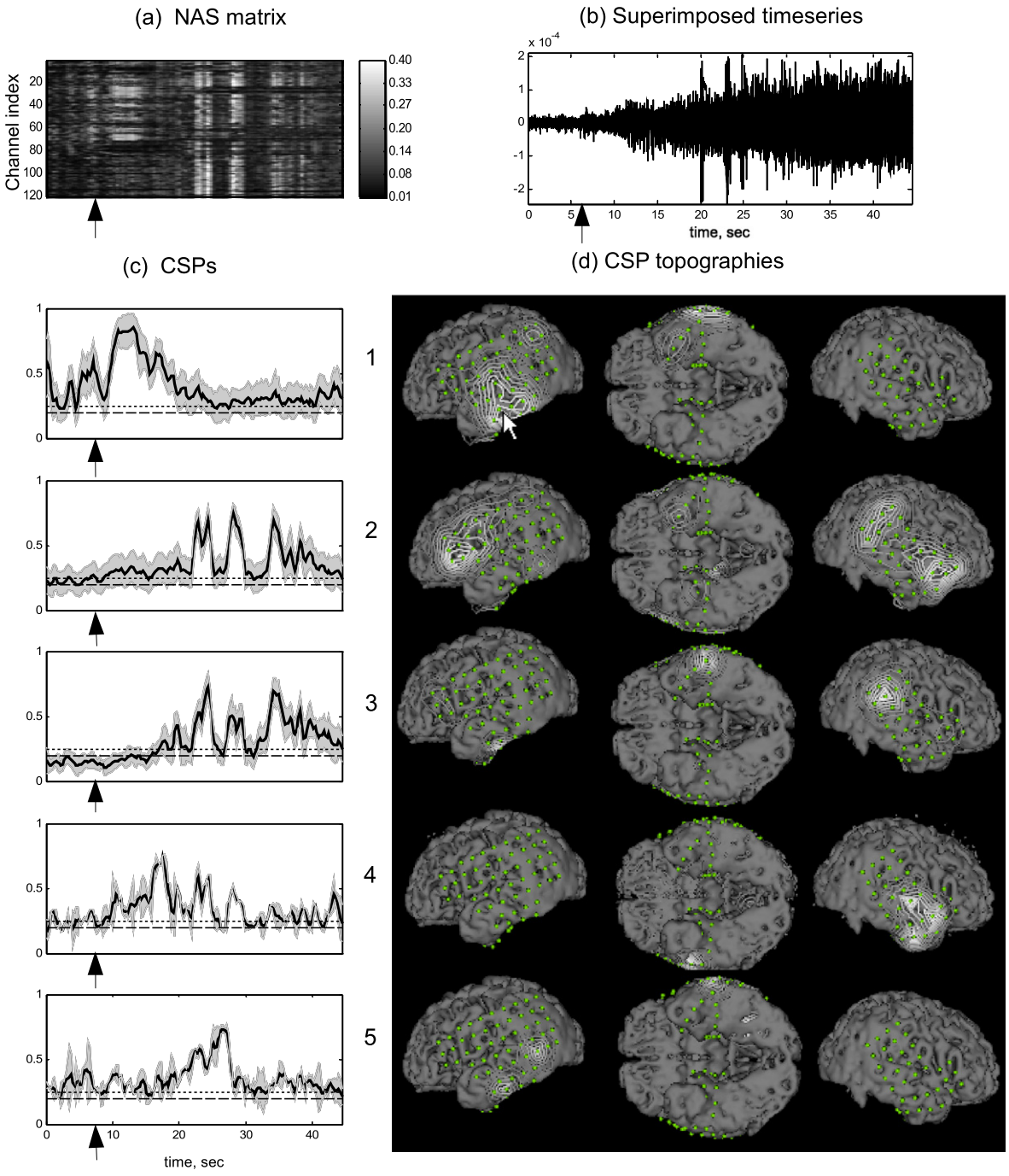

Fig. 9. The results of CSP (c)+ NAS (a) analysis are shown for seizure transition interval data segment (b) for Patient 1. The NAS matrix (b) demonstrates the evolution of integral PLV associated with each electrode. Five distinct principal synchrony profiles (CSPs) (c) were identified in the segment. The grey bands correspond to ±1 standard deviation, computed within the corresponding cluster, dashed and fine dashed lines reflect 0.05 and 0.01 significance quantiles for PLV values computed under similar conditions (band-width, averaging interval) but for surrogate non-phase locked signals. CSP topographies (d) represent the degree of involvement of electrodes in their respective CSP. Dots indicate recording sites (electrodes) and white arrow (fifth topography plot on the left) indicates the electrode identified as within the SOZ by an epileptologist, based on the conventional visual analysis of ECoG data. Vertical arrows indicate the seizure onset latency as determined by visual inspection of the ECoG time series data.

sult is partly consistent with those reported by Mormann et al. (2000). A similar pattern was observed in Patients 2 and 3 as it is seen on Figs. 10(a) and 11(a).

The result of the network analysis for Patient 1 is shown in Fig. 9 where five CSP's along with the corresponding topographies may be seen. One of the networks (CSP-1) develops relatively early during seizure onset. The topography of this network overlaps the clinically determined seize onset zone (Fig. 11, SOZ, white arrow). The analysis also identified several other seizure-related networks, including medial temporal/limbic (CSP-4) and superior frontal and contralateral fronto-parietal networks(CSP-2). CSP-3 coresponds to cross-hemispheric parieto-temporal network.

CSPs and the corresponding topographies for patient 2 are shown in Fig. 10. The principal synchronization networks for this patient include left mesial temporal, bilateral mesial temporal, and left frontal–parietal. The patient had a class III outcome after

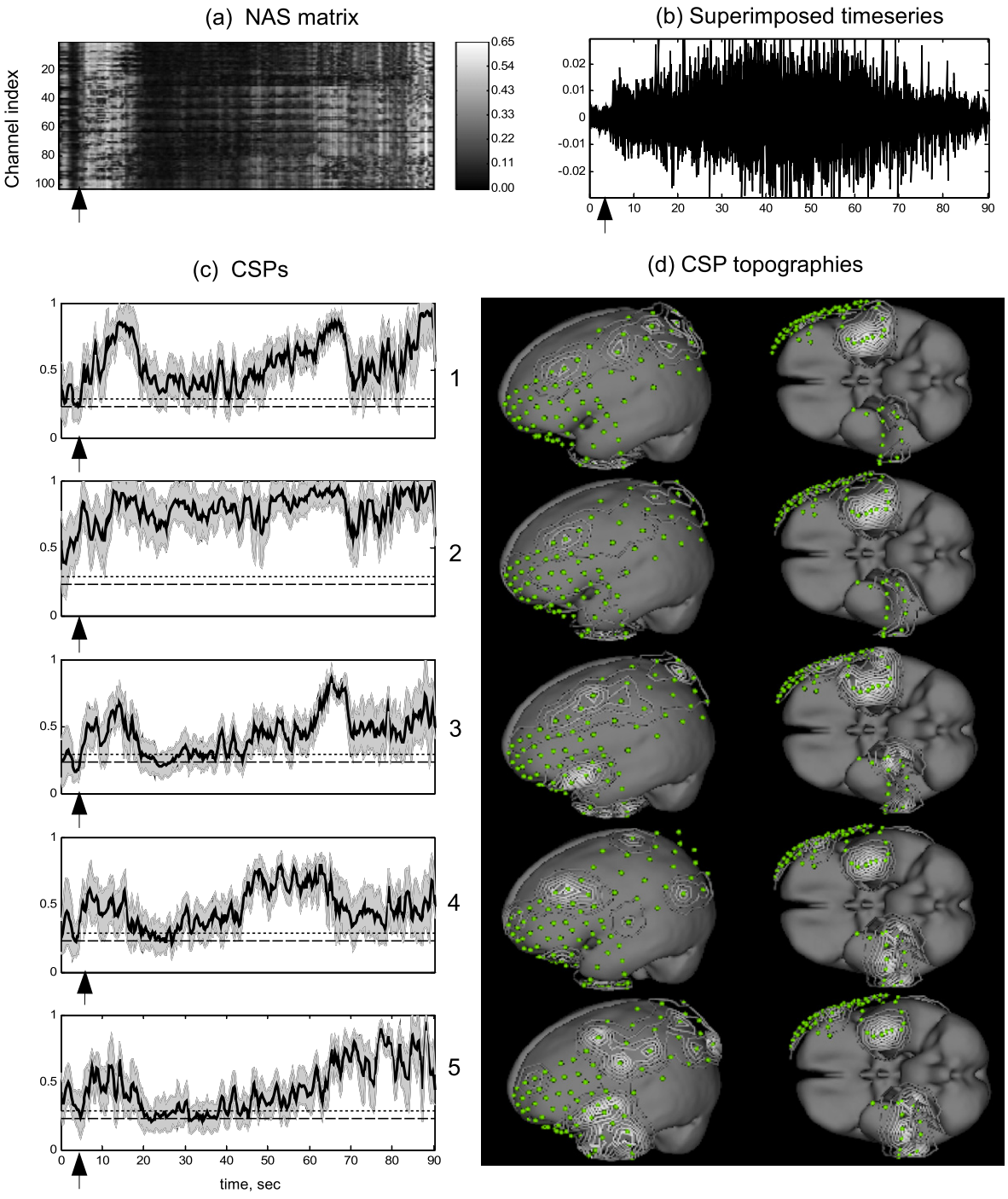

Fig. 10. The results of CSP (c and d) and NAS (a) analysis are shown for the entire seizure interval data segment (b) for Patient 2. The NAS matrix (a) demonstrates the evolution of integral PLV associated with each electrode, (c) illustrates the composite synchrony profiles and their corresponding CSP topographies are shown in (d). Vertical arrows indicate the seizure onset latency as determined by visual inspection of the ECoG time series data.

left parietal and left frontal resection. Because of the poor surgical outcome, it is difficult to interpret the network dynamics with regard to the clinical findings. It is noteworthy, however, that this patient showed significant mesial temporal network nodes on the left (networks 1–3) and bilaterally (networks 4–5), suggesting the possibility that the actual seizure onset zone may have been in the left mesial temporal cortex.

Three independently recorded seizures from Patient 3 were studied by network analysis. The results are illustrated in Fig. 11 While each seizure appears to have distinct network dynamics (visible both in the electrical recordings themselves, the normed aggregate synchrony matrices, and the network results), network analysis revealed both similarities and differences between the seizures.

Each of the seizures show a network with activation beginning at or near seizure onset, with activity in left mesial temporal cortex (1.2, 2.2, 3.4), coincident with the clinically identified seizure onset zone. However, the associations between mesial temporal cortex and other recording locations varied from seizure to seizure. The mesial cortex was associated with a frontal/parietal/inferior tem-

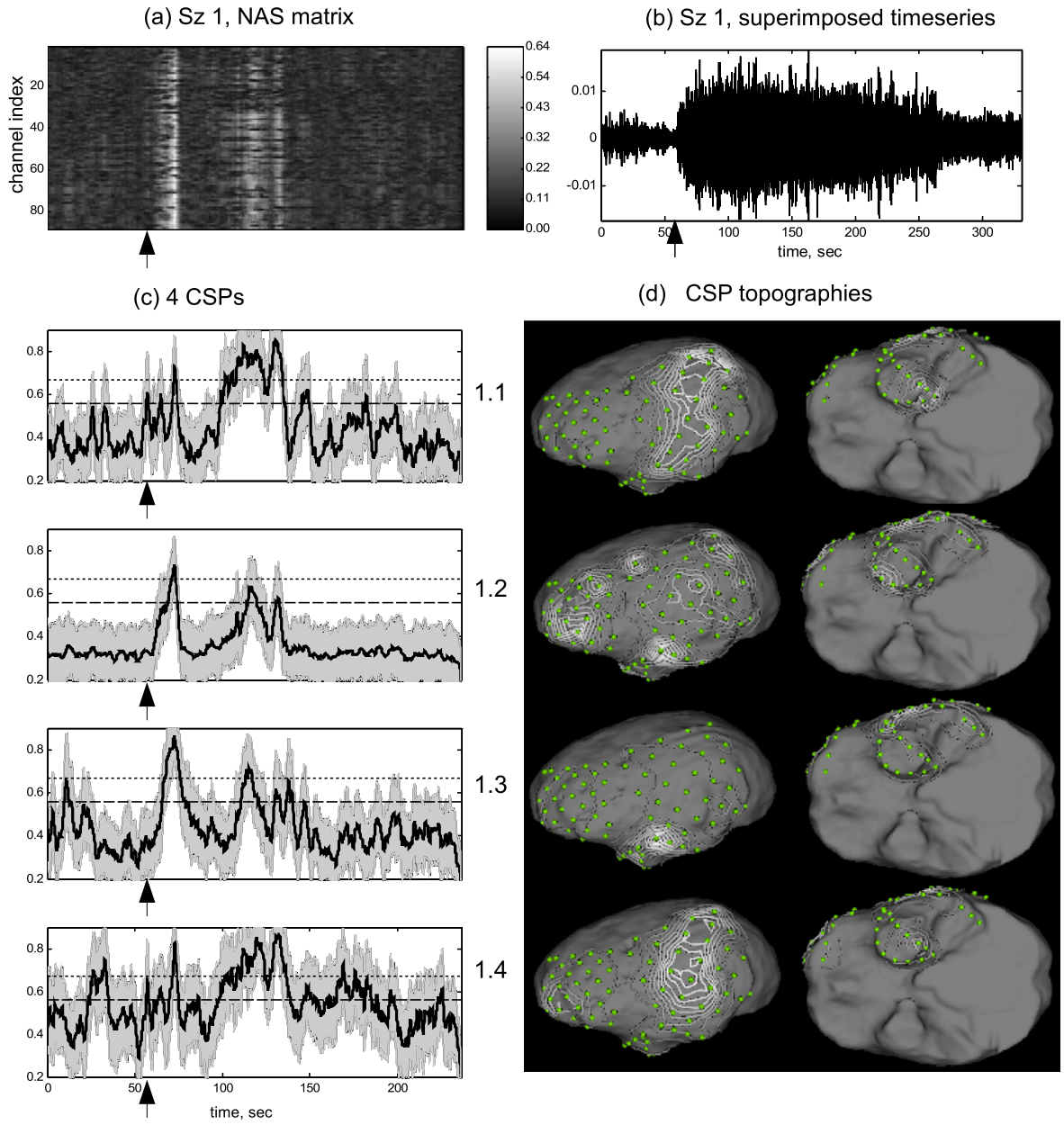

Fig. 11. The results of CSP and NAS analysis as applied to three independently recorded seizures from a Patient 3 are shown in subfigures A–C. In each subfigure (a) illustrates the NAS matrix, computed for the timeseries segment (b), (c) shows the composite synchrony profiles and (d) represents the corresponding CSP topographies. See legend for Fig. 9 for additional details.

poral network in 1.2 and 2.2. 3.4, by contrast, shows a mesial-inferior temporal network without apparent fronto-parietal activation. Additional networks were identified that had temporo-parietal (1.1, 1.4, 2.1), fronto-parietal (2.4, 3.3) and other (e.g., 3.2) topographies.

4. Discussion

We have described two approaches for managing the large amount of data obtained from the spatially specific synchrony measures, the normed aggregate synchrony matrix, and the composite synchrony profile (CSP). The CSP method is based on two successive clustering steps used to reduce the matrices of PLV to a small number of representative temporal profiles of synchrony evolution along with corresponding topographies indicating the degree of involvement of electrodes into particular CSP. We incorporate statistical tests based on a one-way multivariate analysis of variance (MANOVA) to ensure that our networks are statistically distinct.

By combining relatively straightforward multivariate signal processing techniques, such as phase synchrony, with clustering and statistical hypothesis testing, the methods we describe may prove useful for network definition and identification. We note that the network patterns we observe cannot be discovered from direct visual inspection of the raw time series data, nor are they apparent in voltage-based topographic map sequences. We emphasize the modularity of our approach and its conceptual independence of the interaction measures used. Although for concreteness we based our description on the matrices of phase-locking values (Hoke et al., 1989) different measures of synchrony or information flow direction (Nolte et al., 2008; Mormann et al., 2007) can also be employed.

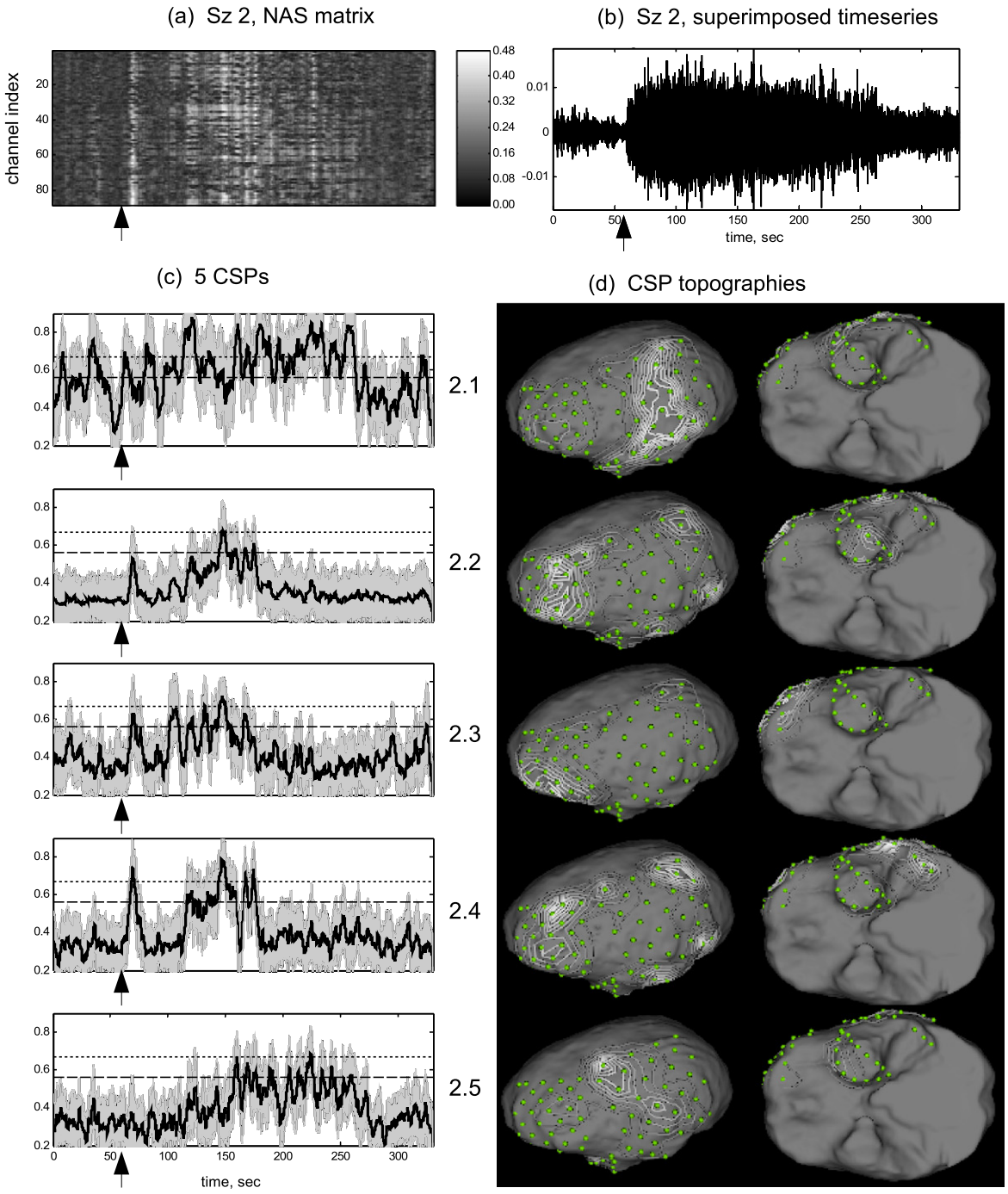

Fig. 11 (*continued*)

The simulations demonstrated that the clustering methods we describe support the extraction of synchrony patterns present in multichannel data, at least when the assumptions of the simulation are attained. The appearance of spurious clusters that have both constant CSPs and topographies involving all of the sensors to essentially equal extents suggests the need for future work to developing appropriate task specific statistical tests to eliminate these special cases.

Application of the clustering technique to clinical ECoG datasets from epilepsy patients revealed a set of distinct CSPs with topographies consistent with medial temporal/limbic and superior parietal/medial frontal networks described in the literature (Spencer, 2002; Bartolomei et al., 2000) as being involved in seizure generation process. For Patient 1 the network corresponding to the earliest synchronization (see Fig. 11, profile #8) is localized to the inferior temporal lobe – the clinically identified epileptogenic zone. For each of the three analyzed seizures from Patient 3, an early-onset network overlapped topographically the clinically determined seizure onset zone.

The results we obtained are complex, and cannot be reduced to a simple picture of seizure dynamics. It seems likely that these diverse network patterns that we observe reflect the real biological diversity of the seizure process (Bergey and Franaszczuk, 2001). The networks we observe include the seizure onset zone, but we

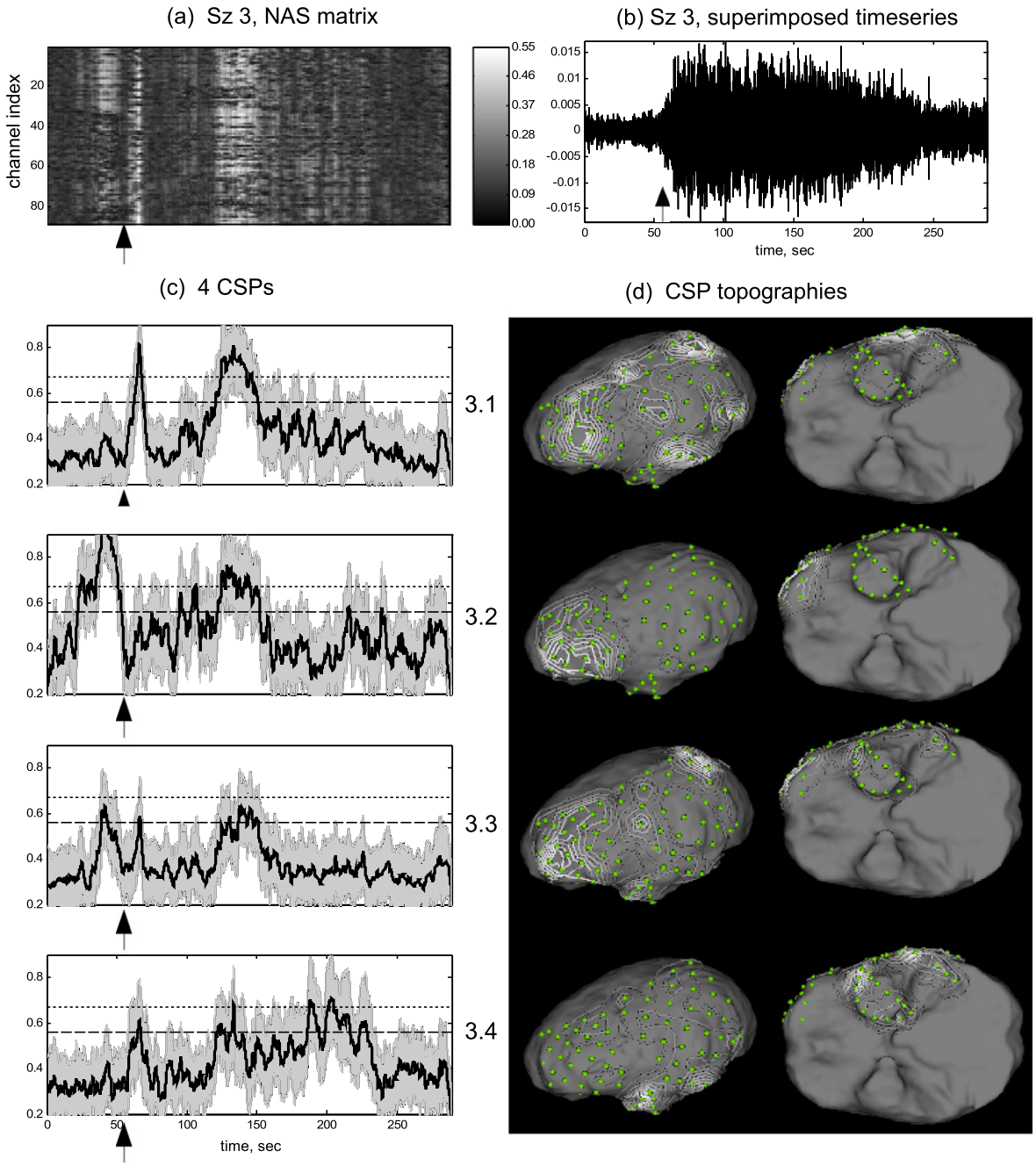

Fig. 11 (*continued*)

do not yet have the means for differentiating between networks to reliably determine which, if any, are involved in the seizure initiation process.

Nevertheless, we believe that these observations constitute a weak validation of the CSP method. That is, the method has shown the ability to reveal statistically significant clusters from patient data, but not that these clusters are predictive of seizure onset. As we show for simulated data, such statistically significant clusters are not a necessary outcome of the clustering procedure. In addition, the identified clusters appear to be physiologically plausible. We have not yet shown that the method is capable of producing clinically relevant results that might aid in surgical management. A stronger validation would require studying a larger patient population with previously identified seizure onset zones and favorable post-surgical outcome.

There exist several other possible methods for reducing the amount of information obtained during bivariate synchrony analysis of ECoG measurements. For example, Allefeld and Bialonski (2007) describe a technique for interpretation of a single synchrony matrix comprised of the PLV values (or possibly other bivariate synchrony measure) for all pairs of channels. The technique is based on reconditioning the observed synchrony matrix into the one that can be interpreted as a transition probability matrix of a Markov Model. Then, using eigenvalue decomposition and clustering, the authors obtain a set of synchronization clusters embedded in the original synchrony matrix. The method as presented is limited to analysis of only a single synchrony matrix.

It is likely that transient networks have lifetimes over a range of time scales, including those a particular significance with characteristic time scales on the order of tens of milliseconds (Friston,

1997). If a single synchrony matrix is computed for a relatively long (several seconds) segment of data it will contain information on the synchronization clusters but will lack sensitivity into the synchrony dynamics, i.e. it will be blind to which clusters are observed during which time subintervals. The extension of the technique described in Allefeld and Bialonski (2007) to the analysis of the matrix of PLV temporal profiles (an $N_{ch} \times N_{ch} \times T$ data structure rather than a single $N_{ch} \times N_{ch}$ synchrony matrix) would require additional clustering step for grouping the time intervals exhibiting similar clusters.

In contrast to the Allefeld et al. method, the CSP approach presented in this paper infers the dynamical nature of synchrony clusters directly and sets as one of its goals the recovery of the temporal dynamics of such transient networks. The use of the terms 'transient networks' and 'transient synchronization clusters' emphasizes the observation that such networks tend to engage and disengage with time on a scale of tens of milliseconds.

Local temporal stationarity is required in order to obtain valid estimates of the CSP synchrony measure. This may hinder application of the CSP method to the purely interictal data. We have not studied the ways to employ the CSP method for seizure prediction purposes.

The CSP method as a technique for efficient bivariate synchrony data reduction is not limited to studying the intracranial recording of seizure onset and may also be used in reducing the synchrony measures obtained from analysis of cognitive neurophysiology experiments to identify the nodes and the dynamics of the networks participating in the large scale integration process (Varela et al., 2001).

Acknowledgments

This work was funded in part by Grant NS049712, U.S. National Institute of Neurological Diseases and Stroke, R.E. Greenblatt, P.I., and in part from funds provided by Source Signal Imaging, Inc. to R.E. Greenblatt and A. Ossadtchi. This study was supported in part by NIH 5 R01 NS40514, The Brain Research Foundation and the Susman and Asher Foundation.

Appendix A. Supplementary methods

A more detailed description of the alogrithms associated with this article can be found, in the online version, at doi:10.1016/j.clinph.2009.12.036.

References

Allefeld C, Bialonski S. Detecting synchronization clusters in multivariate time series via coarse graining of markov chains. Phys Rev E 2007;76(066207).

Bartolomei F, Wendling F, Régis J, Gavaret M, Guye M, Chauvel P. Pre-ictal synchronicity in limbic networks of mesial temporal lobe epilepsy. Epilepsy Res 2000;61(1-3):89–104.

Bergey G, Franaszczuk P. Epileptic seizures are characterized by changing signal complexity. Clin Neurophysiol 2001;12(2):241–9.

Bracewell R. The Fourier transform and its applications. 2nd ed. McGraw-Hill; 1986.

Chang B, Lowenstein D. Mechanisms of disease: epilepsy. NEJM 2003;349(13):1257–66.

Chaovalitwongse W, Suharitdamrong W, Liu C-C, Anderson ML. Brain network analysis of seizure evolution. Ann Zool Fennici 2008;45(5):402–14.

Cohen L. Time–frequency analysis. Prentice-Hall; 1995.

D'Alessandro M, Esteller R, Vachtsevanos G, Hinson A, Echauz J, Litt B. Epileptic seizure prediction using hybrid feature selection over multiple intracranial EEG electrode contacts: a report of four patients. IEEE Trans Biomed Eng 2003;50(5):603–15.

D'Alessandro M, Vachtsevanos G, Esteller R, Echauz J, Cranstoun S, Worrell G. A multi-feature and multi-channel univariate selection process for seizure prediction. Clin Neurophysiol 2005;116(3):506–616.

Esteller R, Echauz J, D'Alessandro M, Worrell G, Cranstoun S, Vachtsevanos G. Continuous energy variation during the seizure cycle: towards an on-line accumulated energy. Clin Neurophysiol 2005;116(3):517–26.

Friston K. Another neural code? Neuroimage 1997;5:213–20.

Hoke M, Lehnertz K, Pantev C, Lükenhoner B. Spatiotemporal aspects of synergetic processes in the auditory cortex as revealed by the magnetoencephalogram. In: Brain Dynamics, Progress and Perspectives, ser. Springer Series in Brain Dynamics. Germany: Springer-Verlag; 1989.

Kondakor I, Toth M, Wackerman J, Gyimesi C, Szopf J, Clemens B. Distribution of spatial complexity of EEG in idiopathic generalized epilepsy and its change after chronic valproate therapy. Brain Topogr 2005;18(2):115–23.

Le Van Quyen M, Soss J, Navarro V, Robertson R, Chavez M, Baulac M. Preictal state identification by synchronization changes in long-term intracranial EEG recordings. Clin Neurophysiol 2005;116(3):559–68.

Mormann F, Addrzejak R, Elger C, Lehnertz K. Seizure prediction: the long and winding road. Brain 2007;130(2):314–33.

Mormann F, Kreuz T, Andrzejak R, David P, Lehnertz K, Elger C. Epileptic seizures are preceded by a decrease in synchronization. Epilepsy Res 2003;53(3):173–85.

Mormann F, Kreuz T, Rieke C, Andrzejak R, Kraskov A, David P. On the predictability of epileptic seizures. Clin Neurophysiol 2005;116(3):569–87.

Mormann F, Lehnertz K, David P, Elger C. Mean phase coherence as a measure for phase synchronization and its application to the EEG of epilepsy patients. Physica D 2000;144(3):358–69.

Nolte G, Ziehe A, Nikulin V, Schlogl A, Kramer N, Brismar T, et al. Robustly estimating the flow direction of information in complex physical systems. Phys Rev Lett 2008;100(23):234101.

Pflieger M, Greenblatt R. Using conditional mutual information to approximate causality for multivariate physiological time series. Int J Bioelectromagnet 2005;7(2):285–8.

Schindler K, Leung H, Elger C, Lehnertz K. Assessing seizure dynamics by analyzing the correlation structure of multichannel intracranial EEG. Brain 2007;130(2):65–77.

Shimizu H, Kawai K, Sunaga S, Sugano H, Yamada T. Hippocampal transection for treatment of left temporal lobe epilepsy with preservation of verbal memory. J Clin Neurosci 2006;13(3):322–8.

Smith M. Multiple subpial transection in patients with extratemporal epilepsy. Epilepsia 1998;39(s4):S81–9.

Spencer S. Neural networks in human epilepsy: evidence of and implications for treatment. Epilepsia 2002;43(3):219–27.

Sporns O, Kotter R. Motifs in brain networks. PLoS Biol 2004;2(11):e369.

Towle V, Carder R, Khorasani L, Lindberg D. Electrocortographic coherence patterns. J Clin Neurophysiol 1999;16(6):528.

Varela F, Lachaux J, Rodriguez E, Martinerie J. The brainweb: phase synchronization and large scale integration. Nat Rev Neurosci 2001;2(4):229–39.

Wennberg R, Arruda F, Quesney L, Olivier A. Preeminence of extrahippocampal structures in the generation of mesial temporal seizures: evidence from human depth electrode recordings. Epilepsia 2002;43(7):716–26.